Supplementary material to: Coupling graphene mechanical resonators to superconducting microwave cavities

P. Weber, J. Güttinger, I. Tsioutsios, D.E. Chang, A. Bachtold[1]

[1]*ICFO-Institut de Ciencies Fotoniques,*

Mediterranean Technology Park, 08860 Castelldefels (Barcelona), Spain

S.1. FABRICATION OF THE SUPERCONDUCTING STRUCTURE

We use a highly resistive silicon substrate (6 kΩcm) with a 295 nm thick, dry chlorinated thermal oxide from *NOVA wafers*. The wafers are sputtered with 200 nm Nb, followed by optical lithography and ion-milling to define the superconducting cavity, the feedline and the graphene contacts. These process steps, and the subsequent wafer dicing, are carried out by *STAR cryoelectronics*. We use Nb as a cavity material because of the high critical temperature $T_c = 9.2$ K that allows the cavity to be tested at liquid helium temperature and to sustain large pump fields. The fine structure of the device, shown in Fig. 1a of the letter, consists of the cavity counter electrode and the support electrodes used later on to anchor the graphene flake. The fabrication of this fine structure is carried out with electron-beam lithography (EBL) and reactive-ion etching (RIE). In a first EBL/RIE step, the cavity counter electrode is separated from the support electrodes. As a mask for etching, we use 50 nm aluminium (Al). The Al-mask is structured with EBL using PMMA and etched in 0.2% Tetra-Methyl-Ammonium-Hydroxide (TMAH) diluted in H_2O. Unmasked areas are cleaned from Al-residues with 30 s ion-milling in an argon (Ar) atmosphere. The Nb is etched with RIE in a 10 mTorr SF_6/Ar atmosphere with a radio frequency (RF) power of 100 W. In a second EBL/RIE step the cavity counter electrode is thinned down, such that the height difference between the cavity counter electrode and the support electrodes equals d.

Here we would like to comment as well on the gap between the two support electrodes, which contact the graphene (Fig. 1a). On the one hand this gap allows measuring electrical transport through the graphene, on the other hand it helps in preventing the collapse of the graphene against the cavity counter electrode during critical point drying. The openings did not show a significant influence on the mechanical behaviour in numeric simulations (private

communication with Andreas Isacsson and Martin Eriksson).

S.2. CHARACTERIZATION OF THE ELECTRICAL SETUP AND THE CAVITY

S.2.1. Calibration of loss and gain in the input and output lines of the cryostat

To relate the externally applied RF power and the measured RF power to the actual fields at the sample, a careful calibration of the attenuation and gain in the setup is needed. The RF-input lines are attenuated at different temperature stages in the cryostat to shield the device from electromagnetic noise and to thermalize the lines. The attenuation is 10 dB at $T = 47$ K, 20 dB at $T = 4$ K, 6 dB at $T = 700$ mK and 20 dB at $T = 30$ mK, where we use for the last attenuation step a directional coupler to physically interrupt the central part of the coaxial line [1]. The total loss in the lines is the sum of the contributions from the attenuators and the loss in cables and connectors. In the input lines of the cold cryostat we measure a total attenuation of $loss(\omega_{\rm d}) = 57$ dB in the 10-100 MHz range and $loss(\omega_{\rm c}) = 64$ dB around $\omega_{\rm c}/2\pi = 6.7$ GHz. The output of the cavity is shielded by two *QUINSTAR CTH0408KC* circulators that are operated as isolators at 30 mK, and then amplified by a low-noise amplifier *LNF-LNC4_8A* from *Low Noise Factory* at 4 K with gain $G(\omega_c) = 43$ dB and noise temperature $T_{\rm noise} \approx 2$ K measured by the factory at 10 K.

We measure a detection limit of $S_{N,SA} = -157$ dBm/Hz in our spectrum analyzer (SA). This noise floor is limited by the input noise of the amplifier. From $k_{\rm B}T_{\rm noise}(G - loss_{\rm 4K-SA}) = -157$ dBm we can extract $G - loss_{\rm 4K-SA} = 38.5$ dB and $loss_{\rm 4K-SA} = 4.5$ dB. The total measured gain of the output line is $gain = G - loss_{\rm 4K-SA} - loss_{\rm sample-4K} \approx 35$ dB with $loss_{\rm sample-4K} \approx 3.5$ dB which is reasonable considering the losses in the two circulators and the line at the level of the sample. Hence we are able to resolve noise powers of $S_{\rm N} > -157$ dBm/Hz-35 dB$= -192$ dBm/Hz in the transmission line of the sample. We measure a total transmitted power of $|S_{21}|^2 = -29.5$ dB in device A and $|S_{21}|^2 = -28.5$ dB in device B, from the output of the RF source to the input of the spectrum analyzer around $\omega_{\rm c}$. This values agree well with our calibration, $|S_{21}|^2 = -loss + gain = -29$ dB.

S.2.2. Analyzing the cavity lineshape

To characterize the external coupling and the internal loss of the cavity, we measure the lineshape of the resonance of the cavity. The normalized transmission is given by [2]

$$S_{21}(\delta\omega_c) = 1 - \frac{\kappa_{ext}/\kappa}{1 + 2i\delta\omega_c/\kappa}. \tag{S1}$$

with $\delta\omega_c$ the detuning from the cavity resonance frequency ω_c, κ the total cavity decay rate and κ_{ext} the external coupling rate of the cavity to the feedline. At resonance ($\delta\omega_c = 0$) the transmission is

$$S_{21,min} = -\frac{\kappa_{ext}}{\kappa_{int}}, \tag{S2}$$

with κ_{int} the internal cavity decay due to cavity internal losses. By measuring the depth and the width of the transmission dip, κ, κ_{ext} and κ_{int} are extracted. In Fig. S1 we show the

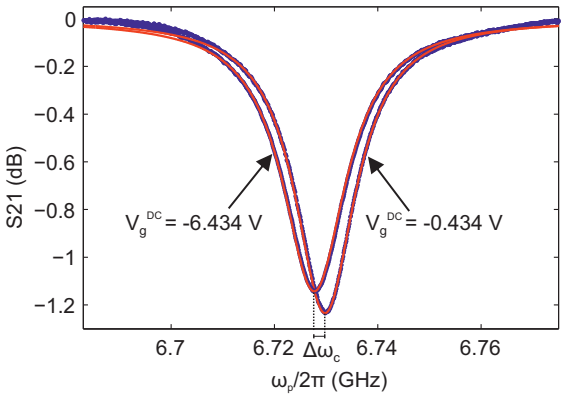

Figure S1. Transmission through the feedline around the cavity resonance frequency.

measured transmission spectrum of device A. For this plot we subtract the background of the measurement containing contributions from the input and the output lines. From a fit of the spectrum to Eq. (S1) we extract for $V_g^{DC} = -0.434$ V the resonance frequency of the cavity $\omega_c/2\pi = 6.73$ GHz and the external and internal decay rates $\kappa_{ext} = 2$ MHz and $\kappa_{int} = 13.2$ MHz. By changing V_g^{DC} to -6.434 V we observe a decrease in the resonance frequency $\Delta\omega_c/2\pi \approx 2$ MHz, which is equivalent to a change in cavity capacitance of $\Delta C \approx 50$ aF. In addition, the internal decay rate of the cavity increases to $\kappa_{int} = 14$ MHz. The change in resonance frequency can be well explained with an increased graphene-cavity capacitance due to static displacement

$$\Delta C_m = \int_0^{2\pi} d\phi \int_0^{R_g} r dr \frac{\epsilon_0}{d - \xi_s(r)} - C_{m0}, \tag{S3}$$

where C_{m0} is the capacitance of the graphene without static displacement at $V_{\mathrm{g}}^{\mathrm{DC}} \approx 0$ V and $\xi_{\mathrm{s}}(r) = z_{\mathrm{s}}(V_{\mathrm{g}}^{\mathrm{DC}}) \cdot (r^2/R^2 - 1)$ (see S.4.2) the static mode shape of the pulled down graphene with $z_{\mathrm{s}}(V_{\mathrm{g}}^{\mathrm{DC}})$ the deflection of the center point of the membrane. If we calculate the capacitive change using $z_{\mathrm{s}}(V_{\mathrm{g}}^{\mathrm{DC}}) = 15$ nm for $V_{\mathrm{g}}^{\mathrm{DC}} \approx 6$ V (Fig. 4a, main text) we obtain $\Delta C_{\mathrm{m}} = 49$ aF. This value is in excellent agreement with the value of ΔC estimated from the change in ω_{c}.

S.2.3. Modeling the dissipation of the cavity

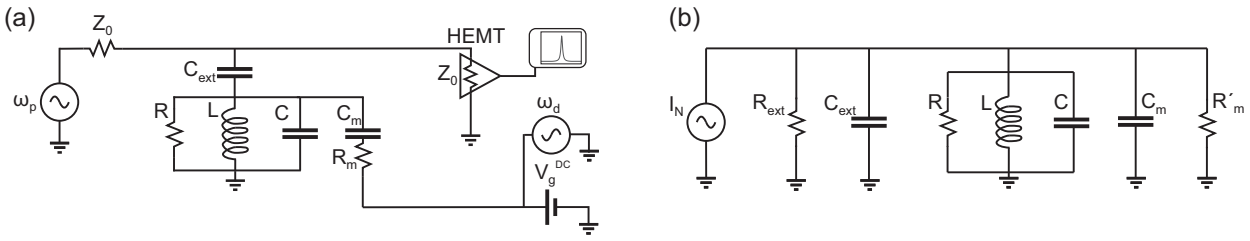

Figure S2. (a) Equivalent circuit of the measurement scheme. (b) Norton equivalent circuit where all the contributions are converted into a parallel RLC circuit.

In Fig. S2a we show a detailed equivalent circuit of our measurement setup. In order to model dissipation we included (i) an input and output impedance of $Z_0 = 50\ \Omega$ in the RF source and the cryogenic amplifier, (ii) a resistor R_{m} for the loss in the graphene and the DC connection and (iii) a resistor R for the internal loss in the cavity. By using a Norton equivalent circuit [3] we can convert all contributions into a parallel equivalent RLC circuit (Fig. S2b) with $1/R_{\mathrm{tot}} = 1/R_{\mathrm{ext}} + 1/R + 1/R'_{\mathrm{m}}$ and $C_{\mathrm{tot}} = C_{\mathrm{ext}} + C + C_{\mathrm{m}}$. We obtain $1/R_{\mathrm{ext}} \approx \omega^2 C_{\mathrm{ext}}^2 Z_0/2$, $I_{\mathrm{N}} = V_{\mathrm{p}} i\omega C_{\mathrm{ext}}$, $1/R'_{\mathrm{m}} \approx \omega^2 C_{\mathrm{g}}^2 R_{\mathrm{m}}$ and we have made use of the fact that in our circuit $\omega C_{\mathrm{ext}} Z_0 \ll 1$ and $\omega^2 R_{\mathrm{m}}^2 C_{\mathrm{g}}^2 \ll 1$. The linewidth of the equivalent parallel RLC-circuit is then given by

$$\kappa = \frac{1}{C_{\mathrm{tot}} R_{\mathrm{tot}}} = \underbrace{\frac{1}{C_{\mathrm{tot}} R_{\mathrm{ext}}}}_{\kappa_{ext}} + \underbrace{\frac{1}{C_{\mathrm{tot}} R}}_{\kappa_{\mathrm{cavity}}} + \underbrace{\frac{1}{C_{\mathrm{tot}} R'_{\mathrm{m}}}}_{\kappa_{\mathrm{g}}} \tag{S4}$$

By substituting the equivalent resistances we get

$$\kappa_{ext} = \frac{\omega_c^2 C_{\mathrm{ext}}^2 Z_0}{2C_{tot}} \qquad \text{and} \qquad \kappa_g = \frac{\omega_c^2 C_g^2 R_m}{C_{tot}}.$$

From the measured external linewidth we estimate the coupling capacitance using the above expression to be

$$C_{\rm ext} = \sqrt{\frac{2C_{\rm tot}\kappa_{\rm ext}}{\omega_{\rm c}^2 Z_0}}.$$

Using $C_{\rm tot} = 90$ fF, $\kappa_{\rm ext}/2\pi = 2$ MHz, $\omega_{\rm c} = 6.7$ GHz and $Z_0 = 50\ \Omega$ we get $C_{\rm ext} = 5$ fF in good agreement with the simulated values of $C_{\rm ext} = 4$ fF for device A and $C_{\rm ext} = 6$ fF for device B.

Furthermore, the measured increase of κ with $V_{\rm g}^{\rm DC}$ in Fig. S1 allows to estimate the resistance R_m in device A. If we assume that the whole change of the linewidth is due to the static displacement of the resonator ($\Delta\kappa = \Delta\kappa_{\rm g}$) we have

$$R_{\rm m} = \frac{\Delta\kappa_{\rm g} C_{\rm tot}}{\omega_{\rm c}^2 (C_{\rm m}^2 - C_{\rm m0}^2)}.$$

Using $\Delta\kappa = \Delta\kappa_{\rm g}$, $\Delta\kappa_{\rm g}/2\pi = 0.8$ MHz, $C_{\rm m} = 0.4$ fF and $C_{\rm m0} = 0.35$ fF (from section S.2.2) we obtain $R_{\rm m} \approx 6$ kΩ. Here, the change in the capacitance $C_{\rm m}$ is derived from the measured change of the cavity resonance frequency $\Delta\omega_c$. By inserting the value for $R_{\rm m}$ in equation (S4) we obtain $\kappa_{\rm cavity}/2\pi = 10.8$ MHz and $\kappa_{\rm g}/2\pi = 2.4$ MHz with $\kappa_{\rm int} = \kappa_{\rm cavity} + \kappa_{\rm g}$. The high value of $\kappa_{\rm int}$ is therefore mainly attributed to the contamination and imperfections of the cavities. Indeed, we have tested the cavity of devices A and B at $T = 4.2$ K before the transfer of the graphene flakes, and we observed larger $\kappa_{\rm int}$ than what we usually observe in devices processed in the same way.

S.3. COUPLING OF THE GRAPHENE RESONATOR TO THE SUPERCONDUCTING CAVITY

S.3.1. Estimation of the coupling parameter g_0

By applying a pump power $P_{\rm p,in}$ at frequency $\omega_{\rm p}$ at the feedline, we create a cavity photon population of

$$n_{\rm p} = \frac{1}{\hbar\omega_{\rm p}} P_{\rm p,in} \cdot \frac{2}{\kappa_{\rm ext}} \cdot \frac{\kappa_{\rm ext}^2}{\kappa^2 + 4(\omega_{\rm p} - \omega_{\rm c})^2}.$$

Here, $\kappa_{\rm ext}/2$ is the coupling of the input mode of the feedline to the cavity and $\kappa_{\rm ext}^2/(\kappa^2 + 4(\omega_{\rm p} - \omega_{\rm c})^2)$ is the lineshape of the cavity resonance. The photon population in the cavity interacts by Stokes (-) and anti-Stokes (+) scattering with the mechanical resonator. The

scattering rates are given by

$$\Gamma_{\pm} = 4n_{\mathrm{p}}g_0^2\frac{\kappa}{\kappa^2 + 4(\omega_{\mathrm{p}} - \omega_{\mathrm{c}} \pm \omega_{\mathrm{m}})^2},$$

with g_0 the single-photon coupling and $\omega_{\mathrm{m}}/2\pi$ the mechanical resonance frequency. In the case of $\omega_{\mathrm{p}} - \omega_{\mathrm{c}} = -\omega_m$ anti-Stokes scattering is resonantly enhanced and we have $\Gamma_{\mathrm{opt}} \approx 4n_{\mathrm{p}}g_0^2/\kappa$ in the so-called resolved sideband limit where $\omega_{\mathrm{m}} \gg \kappa$. Here we introduced Γ_{opt}, the opto-mechanical coupling rate.

The anti-Stokes scattering leads to an equilibrium cavity population n_{c} at ω_{c} determined by $n_c\kappa \approx \Gamma_{\mathrm{opt}}n_{\mathrm{m}}$. Here, we assumed negligible thermal population of the superconducting cavity (at 30 mK $n_{\mathrm{c,th}} = 1/(\exp\hbar\omega_{\mathrm{c}}/k_BT - 1) \ll 1$) and negligible direct population due to the phase noise of the pump. The number of phonons n_{m} is related to the zero-point motion z_{zp} by $n_{\mathrm{m}} \approx \langle z\rangle^2/2z_{\mathrm{zp}}^2$, where $\langle z\rangle$ is the time averaged deflection of the effective mass motion. The cavity mode leaks into the output mode of the feedline with a rate $\kappa_{\mathrm{ext}}/2$ and results in the detectable output power $P_{\mathrm{out}} = n_{\mathrm{c}}\hbar\omega_{\mathrm{c}}\kappa_{\mathrm{ext}}/2$ or

$$P_{\mathrm{out}}(\omega_{\mathrm{c}}) = P_{\mathrm{p,in}} \cdot \frac{\kappa_{\mathrm{ext}}^2}{\kappa^2 + 4(\omega_{\mathrm{p}} - \omega_{\mathrm{c}})^2} \cdot \left(\frac{1}{\kappa}\frac{\partial\omega_{\mathrm{c}}}{\partial x}\right)^2 \cdot 2\left\langle z^2\right\rangle.$$

From the measured output power we can then estimate g_0 as

$$g_0 = z_{\mathrm{zp}}\sqrt{P_{out}(\omega_{\mathrm{c}})\frac{\kappa^2}{n_{\mathrm{p}}\hbar\omega_{\mathrm{c}}\kappa_{\mathrm{ext}}\left\langle z^2\right\rangle}}. \tag{S5}$$

To model the dependence of $g_0 = G_0z_{\mathrm{zp}}$ on the voltage $V_{\mathrm{g}}^{\mathrm{DC}}$ between the graphene and the cavity counter electrode, we have to account for the $V_{\mathrm{g}}^{\mathrm{DC}}$ dependence of both G_0 and z_{zp}. To estimate $G_0(V_{\mathrm{g}}^{\mathrm{DC}})$ we use the calculated value of the equilibrium position z_{s} (Fig. 4a of the letter) to substitute d by $d = d_0 - z_{\mathrm{s}}$ in the calculated graphene-cavity capacitance C_{m}

$$G_0(V_{\mathrm{g}}^{\mathrm{DC}}) = \frac{\omega_c}{2C_{\mathrm{tot}}}\frac{\partial C_{\mathrm{m}}(V_{\mathrm{g}}^{\mathrm{DC}})}{\partial z} \approx \frac{\omega_c}{2C}\frac{0.433\pi R_{\mathrm{g}}^2}{[d_0 - z_{\mathrm{s}}(V_{\mathrm{g}}^{\mathrm{DC}})]^2},$$

where d_0 is the value of d at $V_{\mathrm{g}}^{\mathrm{DC}} = 0$, C_{tot} is the total cavity capacitance approximated by the cavity capacitance C and R_{g} is the radius of the cavity counter electrode. The factor 0.433 is a correction due to the effective mass modeling (see section S.4.4). For the calculation of the capacitance C_{m} see below the section about the effective mass modelling. The increase of the zero-point motion is accounted for by calculating z_{zp} as a function of

$V_{\rm g}^{\rm DC}$ from the measurement of the resonance frequency $\omega_{\rm m}$ as a function of $V_{\rm g}^{\rm DC}$ in Fig. 3c,d of the letter

$$z_{\rm zp}(V_{\rm g}^{\rm DC}) = \sqrt{\frac{\hbar}{2m_{\rm eff}\omega_{\rm m}(V_{\rm g}^{\rm DC})}}.$$

S.3.2. Displacement sensitivity

The detection limit of our readout circuit $S_{\rm N} = -192$ dBm/Hz (see section S.2.1) imposes a limit on the measurement imprecision $\sqrt{S_{\rm z,imp}}$ with

$$S_{\rm z,imp} = \frac{S_{\rm N}\kappa^2 z_{\rm zp}^2}{n_p\hbar\omega_{\rm c}\kappa_{\rm ext}g_0^2}.$$

For the parameters in device A we get $\sqrt{S_{\rm z,imp}} = 2.55$ pm/$\sqrt{\rm Hz}$ at $n_{\rm p} = 8000$ and $\sqrt{S_{\rm z,imp}} = 230$ fm/$\sqrt{\rm Hz}$ at $n_{\rm p} = 10^6$. For comparison, the height of the resonance in the power spectral density of the thermal motion at 1 K is (42 fm/$\sqrt{\rm Hz}$)^2 ((7 fm/$\sqrt{\rm Hz}$)^2 at 30 mK). We will improve our displacement resolution (i) by reducing the loss in the cavity (up to a factor 8 improvement in $\sqrt{S_{\rm z,imp}}$), (ii) by using a quantum limited amplifier [4] (up to a factor 10 improvement in $\sqrt{S_{\rm z,imp}}$) and (iii) by increasing the coupling (with a factor 10 improvement in $\sqrt{S_{\rm z,imp}}$ for $g_0/2\pi = 70$ Hz).

S.4. MECHANICAL MODELLING

S.4.1. Circular graphene resonator in the membrane limit

We model the deflection $\xi(t,x,y)$ of the graphene resonator as a thin plate subject to large external stretching (membrane limit) [5]

$$\rho_{\rm 2D}\frac{\partial^2\xi}{\partial t^2} = T\nabla^2\xi + P(x,y), \tag{S6}$$

with $\rho_{\rm 2D}$ the sheet mass density, $P(x,y)$ the local pressure in z-direction and T a stretching force per unit length at the edge of the membrane. If we consider radially symmetric modes $\xi(t,r)$, the stretching force T is related to a radial strain $\epsilon = (R'-R)/R$ with the elongated radius R' by

$$T = Eh\epsilon = Etn_{\rm g}\epsilon, \tag{S7}$$

with the Young's modulus of graphite $E \approx 1$ TPa or the two dimensional graphene Young's modulus $Et = 340$ N/m [6], n_g the number of graphene layers and $t = 0.335$ nm [7] the interlayer spacing in graphite. The total sheet mass density $\rho_\mathrm{2D} = \eta n_\mathrm{g} \rho_\mathrm{graphene}$ includes the mass from the graphene layers, with the graphene mass density $\rho_\mathrm{graphene} = 7.6 \times 10^{-19}$ kg/μm^2, and a correction factor $\eta \geq 1$ to account for additional adsorbents on the graphene.

The electrostatic pressure due to the gate voltage is modelled in a parallel plate approximation with the capacitive energy given by $U = \frac{1}{2} C_\mathrm{m} V_\mathrm{g}^2$. If we expand the capacitance in terms of ξ we get

$$\begin{aligned} U &\approx \int dxdy \frac{\epsilon_0 V_\mathrm{g}^2}{2} \frac{1}{d - \xi(x,y)} \\ &\approx \int dxdy \frac{\epsilon_0 V_\mathrm{g}^2}{2d} \left(1 + \frac{\xi(x,y)}{d} + \frac{\xi(x,y)^2}{d^2} + \frac{\xi(x,y)^3}{d^3} + \dots\right) \\ \frac{\partial U}{\partial z} &\approx \int dxdy \frac{\epsilon_0 V_\mathrm{g}^2}{2d^2} \left(1 + \frac{2\xi(x,y)}{d} + \frac{3\xi(x,y)^2}{d^2} + \frac{4\xi(x,y)^3}{d^3} + \dots\right) \\ &\approx \int dxdy P(x,y). \end{aligned}$$

The differential equation for the deflection is then given by

$$\rho_\mathrm{2D} \frac{\partial^2 \xi}{\partial t^2} = T\nabla^2 \xi - \frac{\epsilon_0 V_\mathrm{g}^2}{2d^2} \left(1 + \frac{2\xi(x,y)}{d} + \frac{3\xi(x,y)^2}{d^2} + \frac{4\xi(x,y)^3}{d^3} + \dots\right) \tag{S8}$$

To solve the equation, we decompose the deflection $\xi(r,t)$ into a static displacement $\xi_\mathrm{s}(r)$ and time-dependent (radial) modes k with amplitude $\xi_\mathrm{k}(r)$

$$\xi(r,t) \approx \xi_\mathrm{s}(r) + \sum_k \xi_\mathrm{k}(r) e^{-i\omega t}.$$

S.4.2. Static displacement as a function of DC voltage

For the static displacement we have

$$0 = T\nabla^2 \xi_\mathrm{s}(r) - \frac{\epsilon_0 (V_\mathrm{g}^\mathrm{DC})^2}{2d^2} \left(1 + \frac{2\xi_\mathrm{s}(r)}{d} + \dots\right)$$

by assuming $2\xi_\mathrm{s}(r)/d \ll 1$. The solution at lowest order in $\xi_\mathrm{s}(r)/d$ is given by

$$\xi_\mathrm{s}(r) = \frac{\epsilon_0 (V_\mathrm{g}^\mathrm{DC})^2}{8Td^2} \left(r^2 - R^2\right)$$

with the normalized center deflection

$$z_\mathrm{s} = \frac{\epsilon_0 R_\mathrm{g}^2}{8Td^2} (V_\mathrm{g}^\mathrm{DC})^2 = c_\mathrm{s} (V_\mathrm{g}^\mathrm{DC})^2. \tag{S9}$$

For device A, the approximation of small static deflections is well valid up to $V_{\mathrm{g}}^{\mathrm{DC}} \approx 3.5$ V where $z_{\mathrm{s}} = 5$ nm and $2z_{\mathrm{s}}/d = 0.1 \ll 1$. At large $V_{\mathrm{g}}^{\mathrm{DC}}$ we underestimate the static displacement by not including higher order corrections of the electric force. On the other hand we also underestimate the mechanical force when neglecting nonlinear effects as described below. In device B $z_{\mathrm{s}} \approx 7.5$ nm with $2z_{\mathrm{s}}/d = 0.1 \ll 1$, which corresponds to $V_{\mathrm{g}}^{\mathrm{DC}} \approx 5$ V.

The assumption of constant strain at moderate gate voltages is justified by analysing the strain induced by the static deflection. At $V_{\mathrm{g}}^{\mathrm{DC}} \approx 6$ V the additional strain induced by the static deflection of 10 nm (in device B) is given by $\epsilon_{\mathrm{s}} = 2 \cdot 10^{-5} \ll \epsilon_{\mathrm{init}}$, significantly smaller than the initial strain.

S.4.3. Mechanical resonance frequency as a function of gate voltage

If we assume orthogonal modes and neglect mode coupling, we can project Eq. (S8) on the fundamental mode

$$-\rho_{2\mathrm{D}}\omega^2\xi_{\mathrm{f}}(r) = T\nabla^2\xi_{\mathrm{f}}(r) - \frac{\epsilon_0 (V_{\mathrm{g}}^{\mathrm{DC}})^2}{d^3}\xi_{\mathrm{f}}(r) \tag{S10}$$

and solve for the mode amplitude $\xi_{\mathrm{f}}(r)$. Considering a clamped boundary with $\xi_{\mathrm{f}}(R) = 0$ we get

$$\xi_{\mathrm{f}}(r) = \hat{z} J_0\left(\frac{2.4}{R} r\right), \tag{S11}$$

where $\hat{z} = \xi_{\mathrm{f}}(0)$ is the deflection amplitude at the center of the membrane and J_0 is the 0th Bessel function with $J_0(2.4) = 0$. The resonance frequency as a function of gate voltage is then given by

$$\omega_{\mathrm{m}}(V_{\mathrm{g}}^{\mathrm{DC}}) = \sqrt{\frac{2.4^2 T}{R^2 \rho_{2\mathrm{D}}} - \frac{\epsilon_0}{d^3 \rho_{2\mathrm{D}}}(V_{\mathrm{g}}^{\mathrm{DC}})^2}. \tag{S12}$$

By taking into account the reduced radius of the cavity counter electrode R_{g} with respect to the membrane radius R, the electrical force gets reduced by a factor R_{g}^2/R^2 and we obtain

$$\omega_{\mathrm{m}}(V_{\mathrm{g}}^{\mathrm{DC}}) = \sqrt{\frac{2.4^2 T}{R^2 \rho_{2\mathrm{D}}} - \frac{R_g^2}{R^2}\frac{\epsilon_0}{d^3 \rho_{2\mathrm{D}}}(V_{\mathrm{g}}^{\mathrm{DC}})^2} \tag{S13}$$

for the resonance frequency as a function of $V_{\mathrm{g}}^{\mathrm{DC}}$. At $V_{\mathrm{g}}^{\mathrm{DC}} = 0$ V we get in agreement with Ref. [8]

$$\omega_{\mathrm{m}}(0) = \frac{2.404}{R}\sqrt{\frac{Eh\epsilon}{\rho_{2\mathrm{D}}}}.$$

S.4.4. Harmonic oscillator model with effective mass

It is instructive and useful to analyze the dynamics of the resonator by a harmonic oscillator model with an effective mass. From the total kinetic energy

$$E_{\rm kin} = \frac{1}{2}\rho_{\rm 2D} 2\pi \int r\xi_{\rm f}^2(r)dr = \frac{1}{2} m_{\rm eff}\hat{z}^2 \tag{S14}$$

we obtain for the effective mass

$$m_{\rm eff} = 0.27\rho_{\rm 2D}\pi R^2, \tag{S15}$$

with

$$2\pi\int_0^R dr J_0\left(\frac{2.4}{R}r\right) r = 2\pi\frac{R^2}{2.4^2}\int_0^{2.4} dr' J_0(r')r' = 0.27\pi R^2.$$

We multiply all the terms of Eq. (S8) by $J_0\left(\frac{2.4}{R}r\right)$ and integrate over the area. As a result, we get the normalized equation of motion with higher order corrections for the capacitive force

$$\begin{aligned} m_{\rm eff}\omega^2\hat{z} = &\left(0.271\pi R^2 2.4^2 T - 0.271\frac{\epsilon_0\pi R_{\rm g}^2 V_{\rm g}^2}{d^3}\right)\hat{z} \\ &+0.196\frac{3\epsilon_0\pi R_{\rm g}^2 V_{\rm g}^2}{2d^4}\hat{z}^2 \\ &+0.125\frac{2\epsilon_0\pi R_{\rm g}^2 V_{\rm g}^2}{d^5}\hat{z}^3 + \ldots. \end{aligned} \tag{S16}$$

Note that we obtain the same expression as Eq. S13 for the resonance frequency

$$\omega_{\rm m}(V_{\rm g}^{\rm DC}) = \sqrt{\frac{4.92Eh\epsilon}{m_{\rm eff}} - \frac{0.271}{m_{\rm eff}}\frac{\epsilon_0\pi R_{\rm g}^2}{d^3}(V_{\rm g}^{\rm DC})^2} = \sqrt{\frac{2.4^2 T}{R^2\rho_{\rm 2D}} - \frac{R_{\rm g}^2}{R^2}\frac{\epsilon_0}{d^3\rho_{\rm 2D}}(V_{\rm g}^{\rm DC})^2}.$$

S.4.5. Induced motion over capacitive drive

First we are interested in the mechanical response under a weak electrostatic drive, such that nonlinear motional effects can be neglected:

$$m_{\rm eff}\ddot{z}(t) + \gamma_m m_{\rm eff}\dot{z}(t) + m_{\rm eff}\omega_m^2 z(t) = \hat{F}_{\rm d}\cos(\omega_d t). \tag{S17}$$

The damping is characterized by the linewidth $\gamma_{\rm m} = \omega_{\rm m}/Q_{\rm m}$ with $Q_{\rm m}$ the quality factor of the mechanical resonator and ω_m the mechanical resonance frequency. The electrostatic drive amplitude is given by $\hat{F}_{\rm d} = \partial_z C_{\rm m} V_{\rm g}^{\rm DC}\sqrt{2}V_{\rm g}^{\rm AC}$, with $V_{\rm g}^{\rm AC}$ the root-mean-square amplitude

of the drive voltage. Including the capacitive correction for the modeshape from above we have $\hat{F}_\mathrm{d} = 0.433 \cdot \epsilon_0 \pi R_\mathrm{g}^2/d^2 V_\mathrm{g}^\mathrm{DC}\sqrt{2}V_\mathrm{g}^\mathrm{AC}$. With the ansatz $z(t) = \hat{z}e^{i\omega_\mathrm{d}t}$ we get

$$-m_\mathrm{eff}\omega_\mathrm{d}^2\hat{z} + i\gamma_m m_\mathrm{eff}\omega_\mathrm{d}\hat{z} + m_\mathrm{eff}\omega_m^2\hat{z} = \hat{F}_\mathrm{d} \tag{S18}$$

and hence for the amplitude

$$\hat{z}(\omega_\mathrm{d}) = \frac{F_\mathrm{d}/m_\mathrm{eff}}{\sqrt{(\omega_\mathrm{m}^2 - \omega_\mathrm{d}^2)^2 + \gamma_\mathrm{m}^2\omega_\mathrm{d}^2}}. \tag{S19}$$

When driving at resonance $\omega_\mathrm{d} = \omega_\mathrm{m}$, we have

$$\hat{z}(\omega_\mathrm{m}) = \frac{F_\mathrm{d}}{m_\mathrm{eff}\gamma_m\omega_\mathrm{d}}. \tag{S20}$$

S.4.6. Nonlinear lineshape

We include the cubic nonlinear force in the driven equation of motion

$$m_\mathrm{eff}\ddot{z}(t) + i\gamma_m m_\mathrm{eff}\dot{z}(t) + m_\mathrm{eff}\omega_m^2 z(t) + \alpha_\mathrm{eff} z^3(t) = \hat{F}_\mathrm{d}\cos(\omega_\mathrm{d}t). \tag{S21}$$

with α_eff a constant.

In analogy to the linear lineshape in Eq.(S19) we get for the amplitude of the motion

$$\hat{z}(\omega_\mathrm{d}) \approx \frac{\hat{F}_\mathrm{d}/2m_\mathrm{eff}\omega_m^2}{\sqrt{\left(\frac{\omega_\mathrm{d}-\omega_m}{\omega_m} - \frac{3}{8}\frac{\alpha_\mathrm{eff}}{m_\mathrm{eff}\omega_m^2}\hat{z}_0^2\right)^2 + (2Q)^{-2}}}$$

in the limit of small oscillations where $\alpha_\mathrm{eff}\hat{z}^3 < k\hat{z}/Q_\mathrm{m}$ (see Ref. [9] Eq. 1.31a). The onset of bistability is given by [9]

$$\hat{z}_\mathrm{crit} = \sqrt{\frac{8}{3\sqrt{3}}\frac{m_\mathrm{eff}\omega_m^2}{Q\alpha_\mathrm{eff}}} = 1.24\sqrt{\frac{m_\mathrm{eff}\omega_m^2}{Q\alpha_\mathrm{eff}}}. \tag{S22}$$

Thus the Duffing nonlinearity can be calculated from the critical deflection amplitude

$$\alpha_\mathrm{eff} = \frac{8}{3\sqrt{3}}\frac{m_\mathrm{eff}\omega_m^2}{Q_\mathrm{m}\hat{z}_\mathrm{crit}^2}. \tag{S23}$$

S.4.7. Harmonic oscillator with nonlinear contributions and static displacement

We consider quadratic and cubic nonlinear terms in the equation of motion (without dissipation and drive)

$$m_{\mathrm{eff}}\ddot{z}(t) = -m_{\mathrm{eff}}\omega_m^2 z(t) - \beta_0 z^2(t) - \alpha_0 z^3(t) + F_{\mathrm{el}}, \tag{S24}$$

with β_0 and α_0 two constants. With the separation ansatz $z(t) = z_{\mathrm{s}} + z_{\mathrm{f}}(t)$ we get

$$\begin{aligned} m_{\mathrm{eff}}\ddot{z}_{\mathrm{f}}(t) = &- \left[m_{\mathrm{eff}}\omega_{\mathrm{m},0}^2 z_{\mathrm{s}} + \beta_0 z_{\mathrm{s}}^2 + \alpha_0 z_{\mathrm{s}}^3 - \frac{1}{2}\partial_z C_{\mathrm{m}}(z_{\mathrm{s}})V_{\mathrm{g}}^2\right] \\ &- \underbrace{\left[m_{\mathrm{eff}}\omega_{\mathrm{m},0}^2 + 2\beta_0 z_{\mathrm{s}} + 3\alpha_0 z_{\mathrm{s}}^2 - \frac{1}{2}\partial_z^2 C_{\mathrm{m}}(z_{\mathrm{s}})V_{\mathrm{g}}^2\right]}_{k_{\mathrm{tot}}} z_{\mathrm{f}}(t) \\ &- \underbrace{\left[\beta_0 + 3\alpha_0 z_{\mathrm{s}} - \frac{1}{4}\partial_z^3 C_{\mathrm{m}}(z_{\mathrm{s}})V_{\mathrm{g}}^2\right]}_{\beta_{\mathrm{tot}}} z_{\mathrm{f}}^2(t) \\ &- \underbrace{\left[\alpha_0 - \frac{1}{12}\partial_z^4 C_{\mathrm{m}}(z_{\mathrm{s}})V_{\mathrm{g}}^2\right]}_{\alpha_{\mathrm{tot}}} z_{\mathrm{f}}^3(t) \end{aligned}$$

From the first bracket we can estimate the static displacement by neglecting the nonlinear contributions and assuming a similar deflection profile as the fundamental oscillation

$$\begin{aligned} z_{\mathrm{s}} &\approx \frac{1}{2m_{\mathrm{eff}}\omega_{\mathrm{m},0}^2}\partial_z C_{\mathrm{m}}(V_{\mathrm{g}}^{\mathrm{DC}})^2 \\ &\approx \frac{0.433}{2m_{\mathrm{eff}}\omega_{\mathrm{m},0}^2}\frac{\epsilon_0\pi R_g^2}{d^2}(V_{\mathrm{g}}^{\mathrm{DC}})^2 \\ &= \frac{\epsilon_0 R_{\mathrm{g}}^2}{7.21Td^2}(V_{\mathrm{g}}^{\mathrm{DC}})^2. \end{aligned}$$

Compared to the result of the direct calculation with the static modeshape in Eq. (S9) there is a small difference with a factor 7.21 instead of 8 in the denominator. For device B, it is possible to analyze the nonlinear contribution in k_{tot}. For $z_{\mathrm{s}} = 17$ nm the nonlinear contribution equals the linear contribution as $3\alpha_0 z_{\mathrm{s}}^2 = m_{\mathrm{eff}}\omega_{\mathrm{m}}^2 = 1.6$ kg·s^{-2} with $\alpha_0 = 1.9 \times 10^{15}$ kg·s^{-2}m^{-2}.

For small nonlinear amplitudes we transform the quadratic and cubic nonlinear terms in

a single cubic term [10]

$$\begin{aligned}\alpha_{\rm eff} &\approx \alpha_{\rm tot} - \frac{10}{9}\frac{\beta_{\rm tot}^2}{m_{\rm eff}\omega_m^2} \\ &\approx \alpha_0 - \frac{1}{12}\partial_z^4 C_{\rm m}(V_{\rm g}^{\rm DC})^2 - \frac{10}{9m_{\rm eff}\omega_m^2}\left(3\alpha z_{\rm s} - \frac{1}{4}\partial_z^3 C_{\rm m}(V_{\rm g}^{\rm DC})^2\right)^2 \\ &\approx \alpha_0 - \frac{1}{12}\partial_z^4 C_{\rm m}(V_{\rm g}^{\rm DC})^2 - \frac{10}{144m_{\rm eff}\omega_m^2}\partial_z^3 C_{\rm m}^2(V_{\rm g}^{\rm DC})^4 - \frac{10}{m_{\rm eff}\omega_m^2}\alpha_0^2 z_{\rm s}^2.\end{aligned}$$

We assumed that $\partial_z^n C_{\rm m}(z_{\rm s}) \approx \partial_z^n C_{\rm m}(z_{\rm s}=0)$ and that β is small (no symmetry breaking visible at small $V_{\rm g}^{\rm DC}$). With $\alpha_0 = 1.9\times10^{15}$ kg s^{-2}m^{-2} and $V_{\rm g} = 5$ V, the second and the third terms of the last equation are $\approx -6\times10^{12}$kg s^{-2}m^{-2} and $\approx -6\times10^{11}$kg s^{-2}m^{-2} respectively. This is much smaller than the fourth term ($\approx -4\times10^{15}$kg s^{-2}m^{-2}). Hence we can write

$$\alpha_{\rm eff} \approx \alpha_0 - \frac{10}{m_{\rm eff}\omega_m^2}\alpha_0^2 z_{\rm s}^2. \tag{S25}$$

The measured values for the Duffing nonlinearities are within the range of $\alpha_{\rm eff} = 1.74\cdot10^{12}$ kg·m^{-2}s^{-2} to $7.16\cdot10^{17}$ kg·m^{-2}s^{-2} observed in other graphene resonators [11, 12] and are compatible with the observation of intermediate strain.

S.4.8. Heating of the mechanical resonator by large pump fields

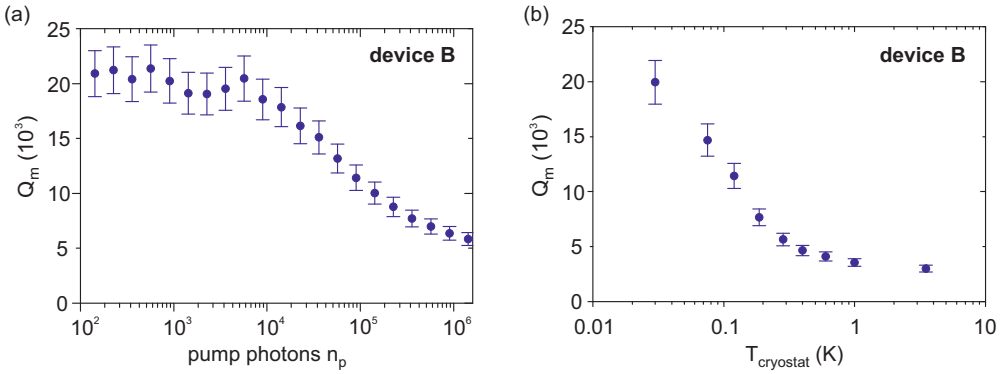

Figure S3. Heating of the mechanical mode by increasing the pump field in device B.

In Fig. S3a we show a measurement of the quality factor in device B as a function of the number of pump photons in the cavity. While the quality factor is roughly constant for $n_{\rm p} < 6000$, $Q_{\rm m}$ decreases for higher pump fields. Upon increasing the temperature of our cryostat $Q_{\rm m}$ also decreases, as shown in Fig. S3b. From the comparison between the

two figures we conclude that a pump power of $n_{\mathrm{p}} = 10^6$ has the same influence on the mechanical resonator as heating the cryostat to 200 mK. In order to minimize the heating it is beneficial to reduce the resistance of the graphene and to improve the heat flow away from the mechanical resonator.

REFERENCES

[1] J. Teufel, T. Donner, D. Li, J. Harlow, M. Allman, K. Cicak, A. Sirois, J. Whittaker, K. Lehnert, and R. Simmonds, Nature **475**, 359363 (2011).

[2] B. A. Mazin, *Microwave kinetic inductance detectors*, Ph.D. thesis, California Institute of Technology (2005).

[3] M. Göppl, A. Fragner, M. Baur, R. Bianchetti, S. Filipp, J. M. Fink, P. J. Leek, G. Puebla, L. Steffen, and A. Wallraff, Journal of Applied Physics **104**, 113904 (2008), cavity fabrication, quality factors.

[4] M. Castellanos-Beltran, K. Irwin, G. Hilton, L. Vale, and K. Lehnert, Nature Physics **4**, 929 (2008).

[5] L. D. Landau, E. Lifshitz, J. Sykes, W. Reid, and E. H. Dill, *Theory of elasticity: Vol. 7 of course of theoretical physics*, 2nd ed. (Pergamon Press, 1970) pp. 61,114.

[6] C. Lee, X. Wei, J. W. Kysar, and J. Hone, science **321**, 385 (2008).

[7] R. Al-Jishi and G. Dresselhaus, Phys. Rev. B **26**, 4514 (1982).

[8] S. Timoshenko, *Vibration problems in engineering* (1974).

[9] R. Lifshitz and M. Cross, Reviews of nonlinear dynamics and complexity **1**, 1 (2008).

[10] A. H. Nayfeh and D. T. Mook, *Nonlinear oscillations* (John Wiley & Sons, 2008).

[11] A. Eichler, J. Moser, J. Chaste, M. Zdrojek, I. Wilson-Rae, and A. Bachtold, Nature Nanotechnology **6**, 339 (2011).

[12] X. Song, M. Oksanen, M. A. Sillanpää, H. Craighead, J. Parpia, and P. J. Hakonen, Nano Letters **12**, 198 (2011).